Universiteit
Leiden
The Netherlands

Blood flow dynamics in the total cavopulmonary connection long-term after Fontan completion

Rijnberg, F.M.

Citation
Rijnberg, F. M. (2023, December 20). *Blood flow dynamics in the total cavopulmonary connection long-term after Fontan completion*. Retrieved from https://hdl.handle.net/1887/3674148

Version:	Publisher's Version
License:	Licence agreement concerning inclusion of doctoral thesis in the Institutional Repository of the University of Leiden
Downloaded from:	https://hdl.handle.net/1887/3674148

Note: To cite this publication please use the final published version (if applicable).

CHAPTER 6

6

Segmental analysis of blood flow dynamics in the TCPC

CHAPTER 6A

Segmental assessment of blood flow efficiency in the total cavopulmonary connection using 4D flow MRI: vortical flow is associated with increased viscous energy loss

Friso M. Rijnberg, Joe F. Juffermans, Mark G. Hazekamp, Willem A. Helbing, Hildo J. Lamb, Arno A.W. Roest, Jos J.M. Westenberg, Hans C. van Assen.

European Heart Journal open 2021

Abstract

Objectives

To study flow-related energetics in multiple anatomical segments of the total cavopulmonary connection (TCPC) in Fontan patients from 4D flow MRI, and to study the relationship between adverse flow patterns and segment-specific energetics.

Methods

Twenty-six extracardiac Fontan patients underwent 4D flow MRI of the TCPC. A segmentation of the TCPC was automatically divided into 5 anatomical segments (conduit, superior vena cava, right/left pulmonary artery (PA) and the Fontan confluence). The presence of vortical flow in the PAs or Fontan confluence was qualitatively scored. Kinetic energy, viscous energy loss and vorticity were calculated from the 4D flow MRI velocity field and normalized for segment length and/or inflow. Energetics were compared between segments and the relationship between vortical flow and segment cross-sectional area (CSA) with segment-specific energetics was determined.

Results

Vortical flow in the LPA (n=6) and Fontan confluence (n=12) were associated with significantly higher vorticity (p=0.001 and p=0.015, respectively) and viscous energy loss rate (p=0.046 and p=0.04, respectively) compared to patients without vortical flow. The LPA and conduit segments showed the highest kinetic energy and viscous energy loss rate, while most favorable energetics were observed in the superior vena cava. Conduit CSA inversely correlated with kinetic energy (r= -0.614, p=0.019) and viscous energy loss rate (r= -0.652, p=0.011).

Conclusions

Vortical flow in the Fontan confluence and LPA associated with significantly increased viscous energy loss rate. 4D flow MRI derived energetics may be used as a screening tool for direct, MRI-based assessment of flow efficiency in the TCPC.

Introduction

The Fontan circulation redirects systemic venous blood flow directly towards the pulmonary arteries (PAs), the so called total cavopulmonary connection (TCPC). Consequently, a relatively non-pulsatile, passive pulmonary circulation is present leading to increased central venous pressure and reduced cardiac output(1, 2), both associated with important morbidity. Computational fluid dynamic (CFD) studies have found correlations between adverse, energy-consuming flow patterns and TCPC geometries and adverse outcome, including an elevated central venous pressure(3), reduced cardiac output(4) and reduced exercise performance(5). Therefore, ideally the geometry of the TCPC needs to maximally conserve the limited available energy in the blood flow to achieve optimal hemodynamics, and inefficient areas may be improved by targeted interventions.

Altered flow patterns have been identified in various TCPC segments(6-9). However, 4D flow MRI is able not only to visualize flow patterns in the TCPC *in vivo*(6, 8-10), but also allows novel, voxel-wise quantitative measurements of energy in the flow, e.g. viscous energy loss(6, 8, 11, 12). Thus, 4D flow can provide insights in the energetic consequences of these adverse flow patterns.

However, the comparison of 4D flow derived TCPC energetics in the heterogeneous Fontan population is subject to unique challenges that requires a standardized analysis approach which is currently not available. For example, part of the TCPC can often not be evaluated due to device-related (e.g. fenestration closure device) artefacts making direct comparison between patients without these devices unfeasible. To study 4D flow MRI derived energetics in the TCPC, a standardized analysis approach is needed that divides the TCPC into multiple anatomical segments: extracardiac conduit, Fontan confluence, the left (LPA) and right PAs (RPA) and the superior vena cava (SVC). This approach allows for the direct comparison of segment-specific energetics between patients and between different segments within a patient, but also allows to compare energetics from serial 4D flow scans within one patient.

The aim of this study was to use an automated, segmental analysis approach to 1) evaluate 4D flow derived energetics within five anatomical segments of the TCPC and 2) correlate adverse flow patterns to blood flow energetics within these segments.

Material and Methods

Twenty-six patients with a previous Fontan operation using an extracardiac conduit were retrospectively selected from a local database containing both clinical (routine follow-up, n=7) and research 4D flow MRI scans (n=19) acquired between 2013-2017 (3T, Ingenia, Philips Healthcare, Best, the Netherlands). 4D flow acquisition details are presented in Supplemental Table 1. All 4D flow MRI acquisitions were performed under free-breathing conditions without the use of a respiratory navigator. All patients in this study had either 1) no fenestration performed during surgery or 2) a closed fenestration, either spontaneously or with the use of a fenestration closure device. Long-term outcome was assessed by reviewing the latest medical records for deterioration in NYHA class, newly-onset tachyarrhythmia or failure of the Fontan circulation (cardiac transplant, protein losing enteropathy, death, Fontan take-down) in April 2021. The study was approved by the Medical Ethical Committee and written informed-consent was obtained from all patients and/or guardians.

Division of the TCPC into standardized segments

A 3D reconstruction of the TCPC, covering the extracardiac conduit, SVC (below the brachiocephalic vein), Fontan confluence and the right- and left PAs, was semi-automatically segmented on magnitude-weighted velocity images at the cardiac phase with highest flow (CAAS, MR Solutions, Pie Medical Imaging, Figure 1A-B). In patients with a fenestration closure device or PA stent in situ, only part of the conduit (distal to the device) or PA (proximal to the stent) was included in the segmentation because of device-related flow artifacts. TCPC segments (RPA, LPA, conduit and SVC) with a centerline length <1.5cm were excluded to ensure a sufficient number of voxels in each segment.

To divide the 3D TCPC segmentation into five standardized anatomical segments, the following steps were required; firstly, vessel centerlines were automatically generated between all vessels (Figure 1A, using in-house developed software(13). Subsequently, the TCPC was automatically divided into five anatomical segments, by clipping the geometry perpendicular to the centerline at the centerline bifurcation points (Figure 1B). The functional caval offset (in millimeter, mm), representing how much conduit and SVC flows are set apart to avoid flow collision, was quantified as the distance between the projection of the bifurcation vectors of the conduit and SVC on a plane between the bifurcation vectors of the RPA and LPA (Figure 1C). The cross-sectional area of the conduit, SVC, LPA and RPA were determined perpendicularly to the centerline at a 1mm interval. The mean CSA of the segment was used and normalized for body surface area (BSA).

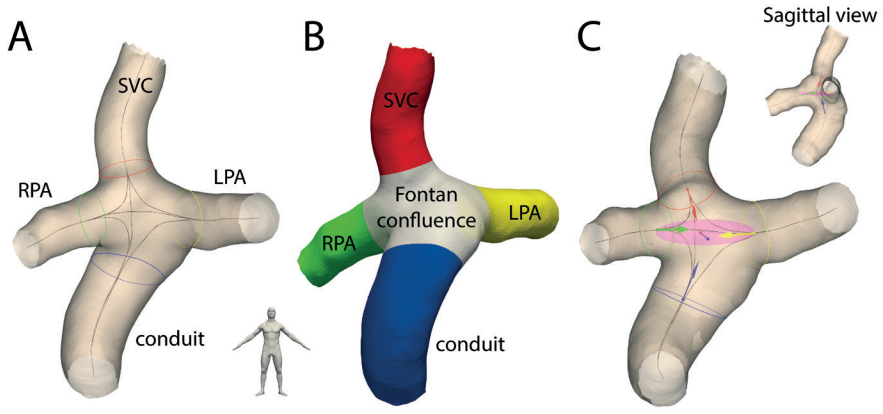

Figure 1. The 3D geometry of the TCPC was automatically divided into 5 anatomical segments by dividing the geometry perpendicular to the centerline (black lines) bifurcation points (colored circles, Figure 1A). The resulting division in 5 anatomical segments is shown in Figure 1B. The functional caval offset (in millimeter, mm) was quantified as the distance between the projection of the bifurcation vectors of the conduit and SVC on a plane (pink) between the bifurcation vectors of the RPA and LPA (Figure 1C).

SVC; superior vena cava, RPA/LPA; right/left pulmonary artery

Qualification of flow patterns

The presence of vortical flow was qualitatively rated within the standardized segments of the Fontan confluence, RPA and LPA. Vortical flow was defined as the presence of a swirling flow >360 degrees in the majority (>50%) of streamlines and/or pathlines. Flow collision between conduit and SVC flow within the Fontan confluence was qualitatively determined, defined as collision of >50% of streamlines/pathlines.

Segments were dichotomized based on the presence/absence of vortical flow (LPA, RPA, Fontan confluence) or caval flow collision (Fontan confluence) and normalized flow energetics (see below) within these segments were compared between the groups. To determine the reproducibility of the qualitative rating of flow patterns, inter-observer analysis was performed on blinded datasets for all cases.

Blood flow energetics

Multiple flow-related energetics were quantified from 4D flow MRI for each voxel within the segments(11, 14). The total amount of each energetic in the different segments was computed for each cardiac phase (25-30 phases per cardiac cycle) by summing voxel-wise energetics within the segment. The cardiac-cycle averaged energetic values were reported. Quantitative energetics included kinetic energy (KE, in millijoules [mJ]), viscous energy loss rate ($\dot{E}L$, in milliwatts [mW]) and vorticity (Vort, in 1/s). KE is the amount of energy present in the blood flow due to motion. $\dot{E}L$ represents the amount

of KE within the blood flow lost per second due to viscosity-induced frictional forces(11, 14). Vorticity represents the amount of spinning motion of the blood flow around a common axis(15). In addition, the proportionality of viscous energy loss to the total amount of KE present during the cardiac cycle was calculated using the dimensionless EL_{index} (EL/KE) as a marker of flow efficiency (16).

Normalization of blood flow energetics

Segmental energetics of the LPA, RPA, SVC and conduit were normalized for inflow rate (in L/min) through each segment and for centerline length of the segment to correct for differences in the extent of the TCPC segmentation (e.g. part of the TCPC can often not be evaluated due to device-related artefacts); $\dot{EL}_{norm_flow+length}$ and $KE_{norm_flow+length}$ in mW and mJ, both per L/min per cm segment, respectively, and $Vort_{norm_flow+length}$ in 1/s per L/min per cm segment. The rationale of the chosen normalization is given in the discussion. The Fontan confluence segment was normalized for flow only (KE_{norm_flow}, EL_{norm_flow} and $Vort_{norm_flow}$) as this segment is always completely included in the segmentation in all patients.

Statistical analysis

Continuous data were presented as median + interquartile range (IQR). Energetics comparisons between segments were performed using the Kruskal Wallis test or Mann-Whitney U test, with post-hoc Dunn's test for multiple comparisons. Inter-observer variability was tested using Cohen's Kappa test (0-0.2 poor, 0.2-0.4 fair, 0.4-0.6 moderate, 0.6-0.8 good, 0.8-1.0 very good agreement. A p-value <0.05 was considered statistically significant. Data were analyzed with SPSS 25.0 (SPSS, IBM Corp., Armonk, NY, USA) and Prism 8.0 (Graphpad Software, La Jolla, CA, USA).

Results

Characteristics of the study population are presented in Table 1. The following number of segments were excluded from analysis: conduit n=12, SVC n=8, LPA n=2, RPA n=4. Main reasons for the exclusion of the segments (centerline length <1.5cm) were the presence of a fenestration closure device (conduit segments, n=13), PA stent (LPA segment, n=1), or because of only a small contribution to the TCPC (RPA and SVC segments). Since the SVC and conduit are often anastomosed close to the hilum of the right lung, the length of the RPA before subdivision into the segmental branches or the length of the SVC below the brachiocephalic vein can be short.

Qualitative flow patterns vs quantitative blood flow energetics

Results of qualitative flow patterns versus quantitative energetics are shown in Table 2-3. Vortical flow was present within the Fontan confluence in 12 patients (46%, Figure 2A, Supplemental video 1), with a significantly higher $Vort_{norm_flow}$ (7746 (IQR 4084) vs 5825 (IQR 2592) per second per L/min inflow, p=0.015) and $\dot{EL}_{norm_flow}$ (0.018 (IQR 0.0073) vs 0.013 (IQR 0.0072) mW per L/min, p=0.046) compared to patients without vortical flow (Table 2).

Table 1. Characteristics of the study population

Male/Female	12/14
Primary diagnosis, n (%):	
HLHS	9 (35)
DILV + TGA	2 (8)
DORV +/- TGA	3 (11)
TA +/- TGA	5 (19)
ccTGA	2 (8)
PA+IVS	2 (8)
Other	3 (11)
Characteristics at 4D flow MRI	
Age (years)	14.4 (4.6, range 10.2-29.2)
Height (cm)	161 (17)
Weight (kg)	47 (21)
BSA (m^2)	1.4 (0.4)
Conduit size (16mm/18mm/20mm)	18/5/3
NYHA class I-II, n (%)	26 (100)
Ejection fraction (%)	51 (8)

Values are presented as median (IQR). MRI; magnetic resonance imaging, BSA; body surface area (Haycock), HLHS; hypoplastic left heart syndrome, DILV; double inlet left ventricle, DORV; double outlet right ventricle, (cc) TGA; (congenitally corrected) transposition of great arteries, TA; tricuspid atresia

Caval flow collision was present in 8 (33%) patients. Patients with caval flow collision had significantly decreased caval offset (2.3mm (IQR 1.2) vs 5.2mm (IQR 3.4), p<0.001). Only 3/8 patients with caval flow collision also showed vortical flow in the Fontan confluence with extension into the LPA in 2 patients. Patients with caval flow collision showed significantly lower KE_{norm_flow}, $\dot{EL}_{norm_flow}$ and $Vort_{norm_flow}$ compared to patients without caval flow collision (Table 2).

Table 2. Comparison of qualitative flow patterns vs quantitative energetics in the Fontan confluence

Energetic	Vortical flow FC (n=12)	No Vortical flow FC (n=14)	P value	Caval flow collision (n=8)	No caval flow collision (n=18)	P value
$Vort_{norm_flow}$	7746 (4084)	5825 (2592)	**0.015**	5224 (2632)	7450 (2608)	**0.011**
KE_{norm_flow}	0.069 (0.036)	0.050 (0.034)	0.053	0.041 (0.019)	0.069 (0.032)	**0.002**
$\dot{EL}_{norm_flow}$	0.022 (0.011)	0.016 (0.013)	**0.046**	0.011 (0.0058)	0.020 (0.0066)	**0.001**
EL_{index}	0.20 (0.09)	0.18 (0.08)	0.35	0.19 (0.04)	0.19 (0.09)	0.94

Values are represented as median (interquartile range). $Vort_{norm_flow}$; vorticity in 1/s per L/min, KE_{norm_flow}; kinetic energy in millijoule per L/min, $\dot{EL}_{norm_flow}$; viscous energy loss rate in milliwatt per L/min. L/min; liter per minute inflow (conduit + superior vena cava flow)

Table 3. Vortical flow patterns versus energetics in the left pulmonary artery

Energetic	Vortical flow LPA (n=6)	No vortical flow LPA (n=18)	P value
$Vort_{norm_flow+length}$	3748 (1380)	2449 (684)	**0.001**
$KE_{norm_flow+length}$	0.032 (0.019)	0.023 (0.015)	0.09
$\dot{EL}_{norm_flow+length}$	0.0085 (0.0058)	0.0060 (0.0035)	**0.04**
EL_{index}	0.19 (0.05)	0.16 (0.06)	0.22

Values are represented as median (interquartile range). $Vort_{norm_flow+length}$; vorticity in 1/s per L/min per cm segment, $KE_{norm_flow+length}$; kinetic energy in millijoule per L/min per cm segment, $\dot{EL}_{norm_flow+length}$; viscous energy loss rate in milliwatt per L/min per cm segment. L/min; liter per minute inflow, LPA; left pulmonary artery

Vortical flow was present in 6/24 LPA segments (Figure 2B, Supplemental Video 2) and 3/22 RPA segments. Patients with vortical flow inside the LPA showed significantly increased $Vort_{norm_flow+length}$, $\dot{EL}_{norm_flow+length}$ and $KE_{norm_flow+length}$ compared to patients without vortical flow (Table 3). No significant differences in energetics could be identified between patients with/without vortical flow in the RPA.

Interobserver agreement was very good for the qualitative rating of caval flow collision and vortical flow in the Fontan confluence (κ=0.91 and 1.0, respectively) and good for the rating of vortical flow in the LPA (κ=0.78) and RPA (κ=0.78).

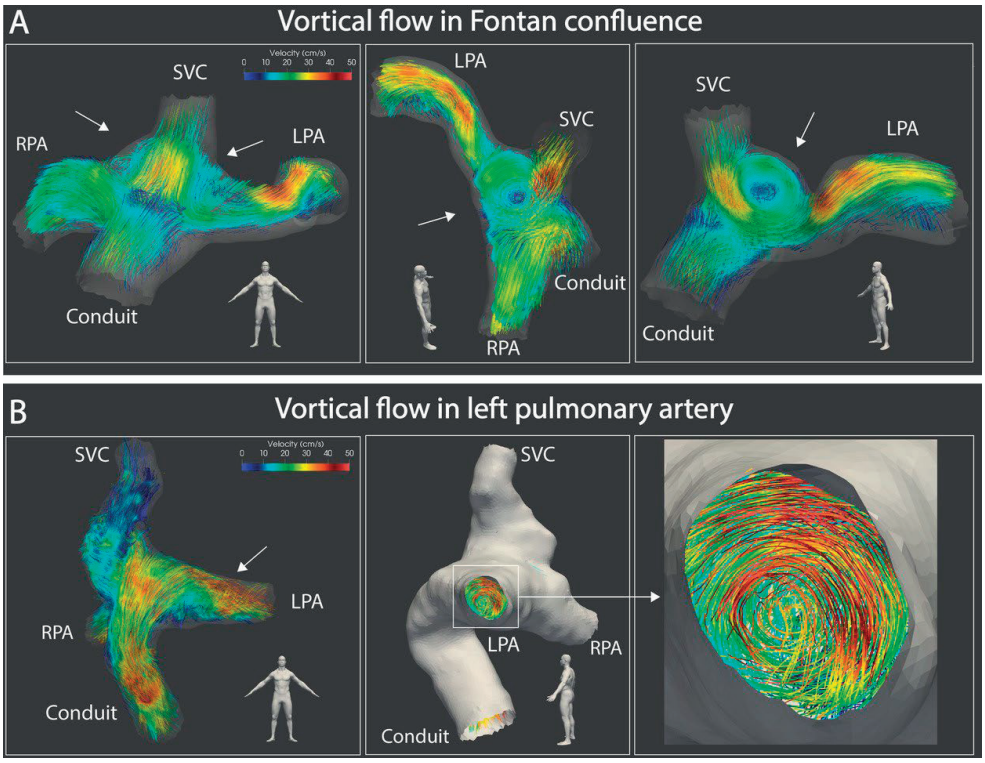

Figure 2. Streamline representation of blood flow in the TCPC is shown from multiple views for 2 patients with a previous Fontan operation using an extracardiac conduit (A-B). (A) A central vortex is shown at the Fontan confluence due to interaction between SVC and conduit flows. (B) Vortical flow is shown in the LPA.

Energetics between TCPC segments

Results of energetics within the different segments are shown in Table 4. $KE_{norm_flow+length}$ was significantly higher in the conduit (0.029 (IQR 0.016)) and LPA (0.025 (IQR 0.013)) compared with the SVC (0.016 (IQR 0.0058) mJ per L/min inflow per cm segment, p=0.004 and p<0.001, respectively). $\dot{EL}_{norm_flow+length}$ was significantly higher in the LPA (0.0060 (IQR 0.0040) compared with the SVC (0.0030 (IQR 0.0023), p<0.001) and RPA (0.0038 (IQR 0.0028) mW per L/min inflow per cm segment, p=0.027). $\dot{EL}_{norm_flow+length}$ in the conduit compared to the SVC did not reach significance (p=0.053). EL_{index} was significantly higher in the FC (0.19 (IQR 0.075)) compared with the RPA (0.14 (IQR 0.050), p<0.001) and conduit (0.15 (IQR 0.083), p=0.041). $Vort_{norm_flow+length}$ was significantly higher in the LPA (2651 (IQR 1273)) compared with the RPA (1714 (IQR 758), p<0.001).

TCPC geometry

The mean CSA/BSA of the conduit, SVC, LPA and RPA are indicated in Table 5. A good inverse correlation was shown between normalized conduit CSA and $KE_{norm_flow+length}$ and

$\dot{EL}_{norm_flow+length}$ and a moderate inverse correlation between normalized RPA CSA and $\dot{EL}_{norm_flow+length}$. Furthermore, a positive correlation was present between normalized LPA CSA and $Vort_{norm_flow+length}$.

Patients with vortical flow in the LPA (n=6) had significantly higher normalized LPA CSA compared to patients without vortical flow (138 (53) vs 94 (50) mm^2/m^2, p=0.014, respectively). Also patients with vortical flow in the RPA (n=3) had significantly higher normalized RPA CSA compared to patients without vortical flow (127 (range 102-172) vs 85 (28) mm^2/m^2, p=0.009, respectively).

Follow-up

Mean follow-up after 4D flow MRI scan was 4.2 (SD 1.1) years. No patients experienced deterioration in NYHA class, newly-onset tachyarrhythmia or failure of the Fontan circulation (cardiac transplant, protein losing enteropathy, death, Fontan take-down).

Table 4. Blood flow energetics in the five anatomical segments of the TCPC

Anatomical segments	$KE_{norm_flow+length}$	$\dot{EL}_{norm_flow+length}$	$Vort_{norm_flow+length}$	EL_{index}
Conduit (n=14)	0.029 (0.016)	0.0059 (0.0040)	2337 (412)	0.15 (0.083)
SVC (n=18)	0.016 (0.0058)	0.0030 (0.0023)	2335 (1204)	0.18 (0.040)
RPA (n=22)	0.023 (0.010)	0.0038 (0.0028)	1834 (658)	0.14 (0.050)
LPA (n=24)	0.025 (0.013)	0.0060 (0.0040)	2651 (1273)	0.17 (0.049)
Fontan confluence (n=26)	-	-	-	0.19 (0.075)

Values are represented as median (interquartile range). $Vort_{norm_flow+length}$; vorticity in 1/s per L/min per cm segment, $KE_{norm_flow+length}$; kinetic energy in millijoule per L/min per cm segment, $\dot{EL}_{norm_flow+length}$; viscous energy loss rate in milliwatt per L/min per cm segment. L/min; liter per minute inflow. $\dot{EL}$, KE and Vort in the Fontan confluence were normalized for flow only and therefore not presented in this table. SVC; superior vena cava, RPA/LPA; right/left pulmonary artery, TCPC; total cavopulmonary connection

Table 5. Correlation between segment cross-sectional area and energetics

		$KE_{norm_flow+length}$		$\dot{E}L_{norm_flow+length}$		$Vort_{norm_flow+length}$		EL_{index}	
Anatomical segment	**CSA/BSA (mm^2/m^2)**	**Correlation coefficient**	**p-value**	**Correlation coefficient**	**p-value**	**Correlation coefficient**	**p-value**	**Correlation coefficient**	**p-value**
Conduit (n=14)	130 (46)	-0.614	**0.019**	-0.652	**0.011**	-0.245	0.399	-0.499	0.069
SVC (n=18)	99 (26)	0.234	0.349	-0.044	0.862	0.335	0.174	-0.117	0.643
RPA (n=22)	89 (31)	-0.338	0.124	-0.440	**0.041**	-0.292	0.188	0.103	0.647
LPA (n=24)	103 (48)	-0.082	0.703	-0.068	0.753	**0.445**	**0.029**	0.252	0.234

Values are indicated as median (interquartile range). Correlation coefficients represent Pearson or Spearman rank analysis. $Vort_{norm_flow+length}$; vorticity in 1/s per L/min per cm segment, $KE_{norm_flow+length}$; kinetic energy in millijoule per L/min per cm segment, $\dot{E}L_{norm_flow+length}$; viscous energy loss rate in milliwatt per L/min per cm segment. L/min; liter per minute inflow. SVC; superior vena cava, RPA/LPA; right/left pulmonary artery, CSA; cross-sectional area, BSA; body surface area (Haycock)

Discussion

This study quantified in vivo 4D flow energetics in a cohort of patients with a previous Fontan operation using an automated analysis approach that divides the TCPC into standardized anatomical segments. Correlations between adverse vortical flow patterns in the LPA and Fontan confluence with quantitative flow-related energetics could be determined. The LPA and conduit segments were the segments with the most inefficient energetics. Furthermore, EL_{index} was highest in the Fontan confluence, indicative that a higher proportion of KE is dissipated at the area where both caval flows meet. Patients with vortical flow in the PA had significantly elevated viscous energy loss, but also significantly larger PA CSA, indicating that PA CSA alone may insufficiently characterize the hemodynamic resistance for pulmonary blood flow. Eventually, this approach may be of interest as a screening tool for direct, MRI-based assessment of flow efficiency in specific segments of the TCPC.

Segmental analysis

In this study, an automated analysis approach was used by subdividing the TCPC into five standardized anatomical segments. This is of importance, as certain parts of the TCPC cannot be evaluated with 4D flow due to device-related artefacts (e.g. stents or fenestration closure devices). Without the applied segmental approach, almost 50% of patients in our study could not have been evaluated with 4D flow energetics due to these device-related artefacts, as these make direct comparison with patients without these devices impossible since inclusion of a larger part of the TCPC will result in higher energetic values. With the segmental approach, the other TCPC segments without artefacts could still be evaluated and compared leading to important insights in segment-specific adverse flow patterns and energetics.

Qualitative flow patterns versus quantitative blood flow energetics

Vortical flow

4D flow MRI has revealed abnormal flow patterns within the TCPC, including helical and vortical flow in the PAs and Fontan confluence(7, 9, 10), at the junction between the IVC and extracardiac conduit(6) or in an attached, blind-ending pulmonary trunk(8). However, how these flow patterns relate to quantitative energetics within these segments with altered flow is not known. In our study cohort, vortical flow was present in the LPA (25%) and Fontan confluence (46%), with significantly higher vorticity compared to patients without vortical flow. The presence of vortical flow was also associated with a significantly higher viscous energy loss rate in these segments. Therefore, as expected, observed vortical flow patterns are related to quantitative 4D flow MRI derived vorticity, and are associated with reduced flow efficiency. The increased $\dot{EL}$ can be explained as

the swirling blood flow leads to increased dissipative velocity gradients (i.e. difference in velocities between adjacent blood elements resulting in energy-dissipating frictional forces) within the blood flow and between the flow and the vessel wall(17).

Vortical flow occurred most often in the LPA which could partially be explained by the presence of a blind-ending pulmonary trunk that was still attached to the LPA in 2 patients, as previously reported(8). Other speculative factors such as interaction of conduit and SVC flow, anastomosis angles and potential influence of the aorta on LPA flow may all play a role but could not be studied in this cohort.

Caval flow collision

Previous in-vitro studies have shown that collision of caval flows result in chaotic, intensely disorganized flow patterns, with helical flow extending into the PAs(18). Incorporating a degree of caval offset resulted in significantly reduced energy loss by avoiding these head collisions of both caval flows(18). In our cohort, caval offset was as expected significantly lower in patients with caval flow collision. Of interest, we surprisingly observed significantly lower $\dot{E}L_{norm_flow+length}$, $KE_{norm_flow+length}$ and $Vort_{norm_flow+length}$ in the Fontan confluence in patients with caval flow collision, at first sight suggesting it to be a favorable flow pattern. However, this is likely not true based on previous obtained results(18, 19) and multiple reasons can contribute to this conflicting result. Most importantly, the relatively low spatial resolution of 4D flow data (see limitations) allows only for assessment of flow patterns on a relatively large scale, and energy-consuming chaotic flow disturbances on a smaller scale, that have been described in the area of flow collision using in vitro models(19), are therefore likely not accounted for. As a result, on a larger scale caval flow collision can cause a decrease in velocity of both caval flows within the Fontan confluence leading to the observed lower energetics. Furthermore, caval flow collision may result in more chaotic flow characteristics in the Fontan confluence with associated turbulent energy losses that are not accounted for by the viscous energy loss metric that assumes laminar flow(14), thereby underestimating total energy loss.

Segment-specific flow energetics

In general, $KE_{norm_flow+length}$ (conduit+LPA) and $\dot{E}L_{norm_flow+length}$ (LPA) were highest in the conduit and LPA, while the SVC had the most favorable energetics. This observation could be due to relatively small diameters of the PA and conduit segments in some patients. CFD studies have demonstrated that the PA and Fontan conduit diameters are the most important factor associated with adverse flow efficiency(20, 21). The velocities in these vessels are often higher, e.g. due to relatively small LPA, often caused by compression by a dilated aortic root, or by the presence of undersized conduits in a proportion of patients leading to increased KE. Significant IVC-conduit mismatch has

previous been shown with 4D flow MRI, especially in adolescent patients with 16mm conduits(6). The increased velocities will lead to stronger velocity gradients between the vessel wall and the peak of the flow profile leading to higher $\dot{E}L$. Interestingly, also patients with higher LPA CSA showed increased $\dot{E}L_{norm_flow+length}$ when vortical flow was present in the LPA, indicating that PA CSA alone may be insufficient to characterize the hemodynamic resistance towards the lung.

The SVC, however, is not restricted as no synthetic material is used and vessel size can adapt to rising flow rates with somatic growth, keeping blood flow velocities and related energetics in the SVC low and favorable. Importantly, clinical decision making regarding the need for intervention is difficult for patients without an evident focal stenosis of the PA or Fontan conduit, but in whom an undersized conduit or overall hypoplastic LPA is present as pressure gradients from catheterization can be absent or minimal. The quantification of segment specific energetics may be helpful to evaluate the significance of these adverse geometries non-invasively.

Overall, the segmental analysis of 4D flow energetics performed in this study illustrates that the LPA and conduit are two important areas in the TCPC that may benefit from optimization by intervention.

Normalization of 4D flow MRI energetics

In order to compare energetics between patients or segments, we chose to normalize energetics in the SVC, conduit, RPA and LPA for inflow and segment length for multiple reasons. Since total energetics are computed using the sum of voxel-wise energetics, total energetics will be influenced by the size of the TCPC. This will be related to the body size of patients, but also by the presence of device-related artefacts that exclude part of the TCPC from 4D flow analysis. Furthermore, under laminar flow conditions, energetics such as $\dot{E}L$ are proportional to flow rate(11, 23), which will differ between patients, but also between different segments within a patient (e.g. the conduit carries 65% of venous return with variable flow splits to both PAs). Therefore, energetics in the SVC, conduit, RPA and LPA were normalized for inflow and segment-length to correct for differences in extent of the segmentation. The Fontan confluence was normalized for flow only, as this segment of the TCPC is always completely available for the analysis. By normalizing energetics in the Fontan confluence for inflow rate, differences in Fontan confluence sizes due to different body sizes will also be corrected for, as flow is considered proportional to BSA(24).

Limitations

The quantification of energetic markers from 4D flow MRI in this study is subject to multiple limitations. Firstly, the spatial resolution of 4D flow is relatively low (2.5mm

isotropic). The absolute amount of viscous energy loss is dependent on the spatial resolution and 4D flow derived viscous $\dot{E}L$ have shown to be orders of magnitude lower compared to "true" CFD-derived values(12). Due to the relatively low spatial resolution, flow phenomena and associated energy losses on a smaller scale are not captured using 4D flow MRI. However, despite measurements of lower energy losses with 4D flow, the relative performance of the TCPC between patients remains intact, thereby still allowing for a relative comparison between patients and most likely also between TCPC segments within patients(12). Furthermore, MRI-related errors such as partial volume artifacts at the vessel borders and the presence of velocity noise will all affect the accuracy of measured velocities and derived energetics. 4D flow protocols have to be optimized for this application, in which optimal compromises between spatial resolution, signal-to-noise-ratio and total scan durations have to be made. Recently, we introduced a non ECG-gated 3D flow MRI sequence (as opposed to ECG-gated 4D flow MRI), allowing for acquisition of cardiac-cycle averaged flow rates and flow rate derived clinical parameters in a <1.5min scan with superior image quality compared to conventional 4D flow MRI.(25)

Importantly, the effect of respiration is not taken into account with the use of 4D flow MRI, thereby not allowing to study the effect of in- and expiration on flow patterns and related energetics. In patients that underwent an Fontan operation, especially conduit flow rate is affected by respiration due to an increase in hepatic venous flow during inspiration(26). However, although respiration influences pulsatility observed in the TCPC, the heart beat is the main driving force for systemic venous return in the Fontan circulation, not affected by respiration(27), which can be adequately captured with the free breathing ECG-gated 4D flow MRI approach used in our study.

Future directions and role on clinical outcome

This cohort represented relatively healthy teenage/adolescent patients after previous Fontan operation that underwent MRI examination as part of routine follow-up, with no events occurring during follow-up. However, the adverse flow patterns present in a subset of patients may provide a chronic burden that may only become apparent later in life. Larger studies with longer follow-up are required to determine its effect on long term outcome, including exercise capacity and degree of liver cirrhosis. Future studies using serial 4D flow scans may provide insights in how segment-specific energetics develop over time, as TCPC blood flow may become increasingly inefficient with time(22), and the proposed standardized segmental approach in this study is important for this serial follow-up.

Conclusions

In conclusion, this study uses a segmental analysis approach to quantify segment-specific 4D flow MRI energetic measurements in the TCPC, allowing for the direct comparison of segment-specific energetics between patients. Furthermore, the segmental approach allows for comparison of energetics between heterogeneous patients with a previous Fontan operation and allow for serial follow-up of hemodynamics using 4D flow MRI. Vortical flow in the Fontan confluence and LPA, observed in 25-46% of patients, was associated with significantly increased viscous energy loss rate. Segmental analysis indicated that the LPA and conduit segments were associated with highest normalized viscous energy loss rate which may be optimized by targeted intervention in these segments. Importantly, patients with vortical flow in the PAs had a significantly larger PA cross-sectional area, indicating that PA CSA alone does not fully characterize the hemodynamic resistance for pulmonary blood flow. 4D flow MRI energetics has the potential to be used as a screening tool for direct, MRI-based assessment of flow efficiency in the TCPC.

References

1. Rijnberg FM, Hazekamp MG, Wentzel JJ, de Koning PJH, Westenberg JJM, Jongbloed MRM, et al. Energetics of Blood Flow in Cardiovascular Disease: Concept and Clinical Implications of Adverse Energetics in Patients With a Fontan Circulation. *Circulation*. 2018 May 29;137(22):2393-407.
2. Gewillig M, Brown SC. The Fontan circulation after 45 years: update in physiology. *Heart*. 2016 Jul 15;102(14):1081-6. PubMed PMID: 27220691. Pubmed Central PMCID: PMC4941188.
3. Sundareswaran KS, Pekkan K, Dasi LP, Whitehead K, Sharma S, Kanter KR, et al. The total cavopulmonary connection resistance: a significant impact on single ventricle hemodynamics at rest and exercise. *Am J Physiol Heart Circ Physiol*. 2008 Dec;295(6).
4. Haggerty CM, Whitehead KK, Bethel J, Fogel MA, Yoganathan AP. Relationship of single ventricle filling and preload to total cavopulmonary connection hemodynamics. *Ann Thorac Surg*. 2015 Mar;99(3):911-7.
5. Khiabani RH, Whitehead KK, Han D, Restrepo M, Tang E, Bethel J, et al. Exercise capacity in single-ventricle patients after Fontan correlates with haemodynamic energy loss in TCPC. *Heart*. 2015 Jan;101(2):139-43.
6. Rijnberg FM, Elbaz MSM, Westenberg JJM, Kamphuis VP, Helbing WA, Kroft LJ, et al. Four-dimensional flow magnetic resonance imaging-derived blood flow energetics of the inferior vena cava-to-extracardiac conduit junction in Fontan patients. *Eur J Cardiothorac Surg*. 2019 Jun 1;55(6):1202-10.
7. Houtzager JH, Westenberg JJ, de Koning PJ, Hazekamp MG, Roest AA. Helical flow pattern in the right pulmonary artery after Fontan palliation. *Eur Heart J Cardiovasc Imaging*. 2014 Oct;15(10):1183.
8. Rijnberg FM, van Assen HC, Hazekamp MG, Roest AAW. Tornado-like flow in the Fontan circulation: insights from quantification and visualization of viscous energy loss rate using 4D flow MRI. *Eur Heart J*. 2019 Jul 1;40(26):2170.
9. Sundareswaran KS, Haggerty CM, de Zelicourt D, Dasi LP, Pekkan K, Frakes DH, et al. Visualization of flow structures in Fontan patients using 3-dimensional phase contrast magnetic resonance imaging. *J Thorac Cardiovasc Surg*. 2012 May;143(5):1108-16.
10. Markl M, Geiger J, Kilner PJ, Foll D, Stiller B, Beyersdorf F, et al. Time-resolved three-dimensional magnetic resonance velocity mapping of cardiovascular flow paths in volunteers and patients with Fontan circulation. *Eur J Cardiothorac Surg*. 2011 Feb;39(2):206-12.
11. Elbaz MS, van der Geest RJ, Calkoen EE, de Roos A, Lelieveldt BP, Roest AA, et al. Assessment of viscous energy loss and the association with three-dimensional vortex ring formation in left ventricular inflow: In vivo evaluation using four-dimensional flow MRI. *Magn Reson Med*. 2017 Feb;77(2):794-805.
12. Cibis M, Jarvis K, Markl M, Rose M, Rigsby C, Barker AJ, et al. The effect of resolution on viscous dissipation measured with 4D flow MRI in patients with Fontan circulation: Evaluation using computational fluid dynamics. *J Biomech*. 2015 Sep 18;48(12):2984-9. PubMed PMID: 26298492.
13. Antiga L, Piccinelli M, Botti L, Ene-Iordache B, Remuzzi A, Steinman DA. An image-based modeling framework for patient-specific computational hemodynamics. *Med Biol Eng Comput*. 2008 Nov;46(11):1097-112.

14. Venkatachari AK, Halliburton SS, Setser RM, White RD, Chatzimavroudis GP. Noninvasive quantification of fluid mechanical energy losses in the total cavopulmonary connection with magnetic resonance phase velocity mapping. *Magn Reson Imaging*. 2007 Jan;25(1):101-9.
15. Fenster BE, Browning J, Schroeder JD, Schafer M, Podgorski CA, Smyser J, et al. Vorticity is a marker of right ventricular diastolic dysfunction. *Am J Physiol Heart Circ Physiol*. 2015 Sep 15;309(6):H1087-93.
16. Kamphuis VP, Westenberg JJM, van der Palen RLF, van den Boogaard PJ, van der Geest RJ, de Roos A, et al. Scan-rescan reproducibility of diastolic left ventricular kinetic energy, viscous energy loss and vorticity assessment using 4D flow MRI: analysis in healthy subjects. *Int J Cardiovasc Imaging*. 2018 Jun;34(6):905-20.
17. Wang C, Pekkan K, de Zelicourt D, Horner M, Parihar A, Kulkarni A, et al. Progress in the CFD modeling of flow instabilities in anatomical total cavopulmonary connections. *Ann Biomed Eng*. 2007 Nov;35(11):1840-56.
18. Sharma S, Goudy S, Walker P, Panchal S, Ensley A, Kanter K, et al. In vitro flow experiments for determination of optimal geometry of total cavopulmonary connection for surgical repair of children with functional single ventricle. *J Am Coll Cardiol*. 1996 Apr;27(5):1264-9. .
19. Amodeo A, Grigioni M, Oppido G, Daniele C, D'Avenio G, Pedrizzetti G, et al. The beneficial vortex and best spatial arrangement in total extracardiac cavopulmonary connection. *J Thorac Cardiovasc Surg*. 2002 Sep;124(3):471-8.
20. Tang E, Wei ZA, Whitehead KK, Khiabani RH, Restrepo M, Mirabella L, et al. Effect of Fontan geometry on exercise haemodynamics and its potential implications. *Heart*. 2017 Nov;103(22):1806-12.
21. Dasi LP, Krishnankuttyrema R, Kitajima HD, Pekkan K, Sundareswaran KS, Fogel M, et al. Fontan hemodynamics: importance of pulmonary artery diameter. *J Thorac Cardiovasc Surg*. 2009 Mar;137(3):560-4. PubMed PMID: 19258065.
22. Restrepo M, Tang E, Haggerty CM, Khiabani RH, Mirabella L, Bethel J, et al. Energetic implications of vessel growth and flow changes over time in Fontan patients. *Ann Thorac Surg*. 2015 Jan;99(1):163-70.
23. Akins CW, Travis B, Yoganathan AP. Energy loss for evaluating heart valve performance. *J Thorac Cardiovasc Surg*. 2008 Oct;136(4):820-33. PubMed PMID: 18954618.
24. Lange PE, Onnasch DG, Schaupp GH, Zill C, Heintzen PH. Size and function of the human left and right ventricles during growth. Normative angiographic data. *Pediatr Cardiol*. 1982;3(3):205-11.
25. Rijnberg FM, van Assen HC, Juffermans JF, Kroft LJM, van den Boogaard PJ, de Koning PJH, et al. Reduced scan time and superior image quality with 3D flow MRI compared to 4D flow MRI for hemodynamic evaluation of the Fontan pathway. *Sci Rep*. 2021 Mar 22;11(1):6507.
26. Hsia TY, Khambadkone S, Redington AN, Migliavacca F, Deanfield JE, de Leval MR. Effects of respiration and gravity on infradiaphragmatic venous flow in normal and Fontan patients. *Circulation*. 2000 Nov 7;102(19 Suppl 3):III148-53.
27. Gabbert DD, Hart C, Jerosch-Herold M, Wegner P, Ravesh MS, Voges I, et al. Heart beat but not respiration is the main driving force of the systemic venous return in the Fontan circulation. *Sci Rep*. 2019 Feb 14;9(1):2034.

Supplementary materials

Supplemental Table 1. 4D flow MRI acquisition details

Respiratory compensation	None (free-breathing)
Cardiac gating	retrospective, 25-30 phases
Spatial resolution (mm)	2.5x2.5x2.5
Temporal resolution (ms)	31.4
Flip angle (°)	10
TE (ms)	3.9
TR (ms)	7.9
VENC (cm/s)	80
Scan duration (minutes)	8-10
Acceleration methods	SENSE factor 2, AP direction EPI factor 5

Typical scan parameters and scan duration are presented.

T; Tesla, ms; miliseconds, TE; echo time, TR; repetition time, VENC; velocity encoding, SENSE; sensitivity encoding, AP; anterior-posterior, EPI; echo planar imaging readout.